remote sensing

MDPI

Technical Note

Evaluating Remote Sensing Metrics for Land Surface Phenology in Peatlands

Michal Antala [1], Anshu Rastogi [1,*], Marcin Stróżecki [1], Mar Albert-Saiz [1], Subhajit Bandopadhyay [1,2] and Radosław Juszczak [1]

[1] Laboratory of Bioclimatology, Department of Ecology and Environmental Protection, Faculty of Environmental and Mechanical Engineering, Poznań University of Life Sciences, Piątkowska 94, 60-649 Poznań, Poland; antala.michal9@gmail.com (M.A.); marcin.strozecki@gmail.com (M.S.); mar.saiz@up.poznan.pl (M.A.-S.); subhajit.iirs@gmail.com (S.B.); radoslaw.juszczak@up.poznan.pl (R.J.)
[2] Centre for Disaster Risk Reduction, School of Internal Security and SMART Policing, Rashtriya Raksha University, Gandhinagar 382305, India
* Correspondence: anshu.rastogi@up.poznan.pl

Abstract: Vegetation phenology is an important indicator of climate change and ecosystem productivity. However, the monitoring of vegetation generative phenology through remote sensing techniques does not allow for species-specific retrieval in mixed ecosystems; hence, land surface phenology (LSP) is used instead of traditional plant phenology based on plant organ emergence and development observations. Despite the estimated timing of the LSP parameters being dependent on the vegetation index (VI) used, inadequate attention was paid to the evaluation of the commonly used VIs for LSP of different vegetation covers. We used two years of data from the experimental site in central European peatland, where plots of two peatland vegetation communities are under a climate manipulation experiment. We assessed the accuracy of LSP retrieval by simple remote sensing metrics against LSP derived from gross primary production and canopy chlorophyll content time series. The product of Near-Infrared Reflectance of Vegetation and Photosynthetically Active Radiation (NIRvP) and Green Chromatic Coordinates (GCC) was identified as the best-performing remote sensing metrics for peatland physiological and structural phenology, respectively. Our results suggest that the changes in the physiological phenology due to increased temperature are more prominent than the changes in the structural phenology. This may mean that despite a rather accurate assessment of the structural LSP of peatland by remote sensing, the changes in the functioning of the ecosystem can be underestimated by simple VIs. This ground-based phenological study on peatlands provides the base for more accurate monitoring of interannual variation of carbon sink strength through remote sensing.

Keywords: climate change; gross primary production; land surface phenology; peatland; vegetation indices

check for updates

Academic Editor: Ruyin Cao

Received: 17 November 2024
Revised: 20 December 2024
Accepted: 24 December 2024
Published: 26 December 2024

Citation: Antala, M.; Rastogi, A.; Stróżecki, M.; Albert-Saiz, M.; Bandopadhyay, S.; Juszczak, R. Evaluating Remote Sensing Metrics for Land Surface Phenology in Peatlands. *Remote Sens.* **2025**, *17*, 32. https://doi.org/10.3390/rs17010032

Copyright: © 2024 by the authors. Licensee MDPI, Basel, Switzerland. This article is an open access article distributed under the terms and conditions of the Creative Commons Attribution (CC BY) license (https://creativecommons.org/licenses/by/4.0/).

1. Introduction

Vegetation phenology plays a key role in the carbon balance of ecosystems and is an essential part of carbon cycle models [1,2]. Because the start of phenological phases is largely dependent on temperature, phenology is one of the most evident climate change indicators [3]. Traditional monitoring of plant phenology is based on the observations of plant organ emergence and development. Sophisticated phenology scales, such as BBCH (Biologische Bundesanstalt, Bundessortenamt und CHemische) or Zadoks, were

developed for agricultural, horticultural, and forestry crops and help to precisely identify the ontogenetic state of plants [4,5]. Nonetheless, phenology monitoring based on personal observations of plants is not suitable for monitoring large ecosystems and remote areas due to huge monetary and personal requirements. However, the phenology measurement for large and distant areas can be supported by satellite remote sensing vegetation indices (VIs). The short revisit time allows for the retrieval of VIs time series and phenology estimation. Nevertheless, due to the presence of clouds in the satellite images, the gaps in the time series have to be filled by smoothing approaches before the phenology retrieval [6]. The retrieved phenology is termed "land surface phenology" (LSP) and is different from the traditional one, as a pixel of a satellite image contains many plants and, in natural ecosystems, many coexisting species with different phenologies [7,8]. Therefore, vegetation phenology is not described as a precise change in ontogenesis but characterizes either the changes in canopy greenness and structure or canopy photosynthetic activity [2]. LSP is mostly limited to the assessment of a few phenological metrics, namely the start of the season (SoS), the peak of the season (PoS), the end of the season (EoS), and the length of the season (LoS). The start and end of the season may be retrieved by several methods that can be grouped into thresholds and curve inflection points. Because the inflection point method is used with logistically fitted curves that assume a simple transition from one state to another, they are mostly suitable for homogeneous vegetation, e.g., crops. Among threshold methods, the dynamic threshold is more versatile compared to the fixed threshold, as the former establishes the day of SoS and EoS based on the local minimal and maximal VI values rather than the fixed value of VI [9–11].

Among a plethora of VI, few are commonly used for LSP retrieval. The Normalized Difference Vegetation Index (NDVI) and Enhanced Vegetation Index (EVI) are the most used VIs for the satellite remote sensing of LSP due to their relation to biomass and chlorophyll content of plants [11]. Simple RGB camera-derived indices, such as Green Chromatic Coordinates (GCC) or Excess Green (ExG), are often used for phenology observation by so-called phenocameras (phenocams). These indices can also be used for satellite remote sensing, as most of the satellites provide red, green, and blue channels [12]. The Plant Phenology Index (PPI) was specifically developed for high-latitude LSP retrieval as it overcomes problems with SoS and EoS estimation related to snowmelt and snowfall [13]. However, other simple VIs that were shown to relate well with canopy chlorophyll content (CCC) or photosynthesis, such as the MERIS Terrestrial Chlorophyll Index (MTCI) and the Near-Infrared Reflectance of Vegetation (NIRv), may be used for LSP retrieval [14,15].

Although substantial research has been done on LSP, studies have mainly focused on croplands and forests, and only little attention has been paid to peatlands in this regard, despite their crucial role in a global carbon cycle. Thanks to their persistent accumulation of partially decomposed organic matter, they contain around a third of the world's soil carbon, although covering only 3% of the land surface of the planet [16]. The underrepresentation of peatlands in LSP research can be attributed to several challenges resulting primarily from the peculiar vegetation. Peatland flora consists of unique species adapted to water-logged, low pH, and low nutrient content conditions [17]. Despite the number of species growing in peatlands being rather low, they differ in terms of morphology, chlorophyll content, overwintering strategy, and temperature requirements for physiological activity [18] (Supplementary Materials S1: Figure S1). Peat mosses (*Sphagnum* spp. L.) form the bottom-most layer of the vegetation and are a crucial component in the majority of northern mires. They overwinter as green, red, or brown plants, depending on the concentration of protective pigments, and start to be photosynthetically active immediately after thawing when the temperature rises above 0 °C [19,20]. Evergreen and deciduous shrubs and herbaceous species start their physiological activity when the temperature crosses a

species-specific threshold. Deciduous species must first develop leaves, which causes a delay in canopy greenness change behind the photosynthetic activity increase. On the contrary, evergreen species photosynthesis starts sooner than their biomass increment [21,22]. Graminoids overwinter in the form of underground storage organs and develop green leaves in the spring. However, their dry leaves from the previous year cover the underlying vegetation in the spring and stay part of the canopy for a significant period of the vegetation season [21] (Supplementary Materials S1: Figure S1). The exact vegetation composition of the peatland and the vegetation community differs from pixel to pixel, which may cause great variability in LSP within a small area.

Existing studies have focused on peatland vegetation phenology retrieved from eddy covariance, phenocam data, or satellite data using only a single VI, assuming that it is the correct VI for the purpose [23–28]. Ground-based (or proximal) spectral measurements are necessary for the assessment of LSP retrieval from different VIs before the use of satellite data because of all the specifics of the peatland vegetation and the fact that the choice of VI significantly affects the retrieved LSP [29,30]. Therefore, we used the hyperspectral reflectance data acquired at the experimental site in central European peatland, where plots of two peatland vegetation communities are under climate manipulation experimentation. We aimed to evaluate the accuracy of the remote sensing metrics in assessing the peatland vegetation's physiological and structural phenology. As the study was performed at the climate manipulation experiment sites over two years with different temperature regimes, the secondary objectives were the determination of the impact of (a) warming (W) and warming and reduced precipitation (WP), (b) the vegetation community, and (c) the natural variation in weather patterns on peatland vegetation phenology with the focus on changes in the physiological and structural phenology.

2. Material and Methods

2.1. Experimental Site

The data used in this study were collected in the years 2019 and 2021 in the climate manipulation experiment on Rzecin peatland (52°45′41″N, 16°18′35″E, 54 m a.s.l.), in western Poland (Figure 1). The experiment consisted of two sites named after the dominant sedge species, CL (after *Carex lasiocarpa* Ehrh.) and CR (named after *Carex rostrata* Stokes). The CL site experiences higher water table depth fluctuation during the year than the CR site, which is located on a floating mat. The vegetation at both sites consists of a mixture of peat mosses, cranberry shrubs, and sedges in different ratios, with a considerable presence of horsetail at the CL site. The share of cranberry shrubs and peat mosses is generally higher at the CR site than the CL site [31,32].

Each of the sites comprised three different treatments in triplicates (all in all, nine plots per site). The treatments included the control (C; with only a collar inserted into the peatland), W (induced only by open-top chambers; OTC) as per Górecki et al. [31] in 2019, the combination of OTC and infrared heaters in 2021 as per Antala et al. [32], and WP (with rain curtains reducing the nighttime precipitation in addition to W).

Radiation-shielded thermohygrometers, HygroVue5 (Campbell Scientific, Logan, UT, USA), were installed next to plots 30 cm above the ground to measure air temperature and relative humidity. Thermohygrometers for the W and WP plots were installed inside the OTCs. The data were recorded every 30 min by datalogger CR1000 (Campbell Scientific, USA). All readings per day for all three plots were used to calculate the daily average for the treatment and the site [31].

Rain gauges TPG-124-H-24 (A-STER, Kraków, Poland) were installed at each site to measure the precipitation amount. The precipitation reduction for the WP plots was calcu-

lated based on the nighttime precipitation when the rain curtains were opened (covering the plots) [31].

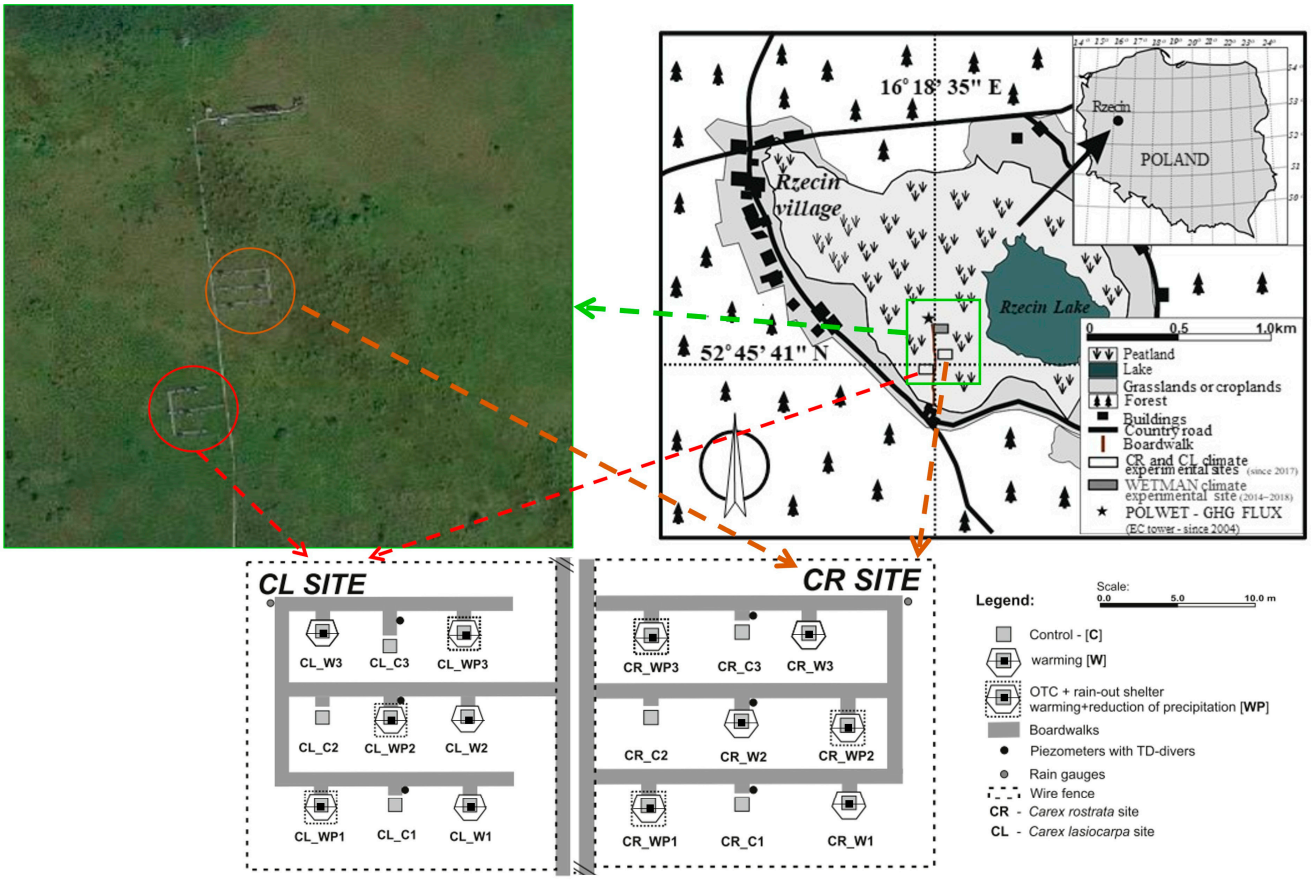


Figure 1. The location of the Rzecin peatland in Poland and the location and experimental design of the CL and CR sites and their plots (part of the figure was adapted from Górecki et al. [31], CC BY-NC-ND license).

2.2. Hyperspectral Data and Vegetation Indices

The hyperspectral data were collected around midday on sunny days (Supplementary Materials S1: Table S1) using a HandHeld 2 spectroradiometer (Malvern Panalytical, Malvern, UK). The spectral range of a HandHeld2 is 325–1075 nm, with a sampling interval of 1.5 nm and a spectral resolution < 3 nm. Five measurements were taken around the center of each plot 1 m above ground distance. As the spectroradiometer's field of view is 25°, the footprint of each measurement had a diameter of 44 cm. Because all the measurements of the day were taken under sunny conditions within 1 h, the integration time was optimized using a Spectralon calibration panel once at the beginning of measurements. A reading of irradiance was taken over the Spectralon panel immediately before every plot measurement. The data were pre-processed in dedicated software, HH2 Sync Version number: 1.3 (Malvern Panalytical, UK), and the reflectance spectra with 1 nm intervals were exported. Subsequently, the following VIs (Supplementary Materials S1: Table S2) were calculated according to references: NDVI [33], NIRv [14], EVI [34], PPI [13], GCC [12], ExG [12], and MTCI [15].

2.3. Carbon Flux Measurements and Gross Primary Production Modeling

A closed dynamic portable chamber system with a transparent chamber for net ecosystem exchange (NEE) and an opaque chamber for ecosystem respiration (Reco), as described by Acosta et al. [35] and Juszczak et al. [36], was used to measure CO_2 fluxes from all exper-

imental plots. The measurements were carried out on days with stable light conditions all year round (Supplementary Materials S1: Table S3) from early morning to late afternoon for all plots at both sites on the same day. The maximum closure time for NEE measurements was 1.5 min, and for Reco measurements, it was 2.5 min. During one day, three in winter to five in summer, complete rounds of measurements were taken for each site, resulting in 54 to 90 flux rate estimations per site.

NEE and Reco were calculated on the basis of CO_2 concentration change in the chamber headspace during the closure time, as described by reference [37]. Gross primary production (GPP) was calculated for each plot as a sum of consecutively measured NEE and Reco, as in Sakowska et al. [38]. A Michaelis-Menten kinetic rectangular hyperbolic light response model was built for every plot and campaign, based on the GPP rates and photosynthetically active radiation (PAR) measured at the time of the NEE measurements [37]. If there were less than four measurements per plot during the campaign, data from two subsequent campaigns were merged. The model parameters were subsequently used to calculate the GPP based on the PAR measured with 30-min time steps. Daily GPP was obtained by summing the half-hourly values over the daylight period (PAR > 20 $\mu mol \cdot m^{-2} \cdot s^{-1}$). The model parameters were linearly interpolated to model the GPP between campaigns, and the half-hourly and daily GPP were estimated as described above.

2.4. Canopy Parameters Modeling

The leaf area index (LAI; $m^2 \cdot m^{-2}$) and CCC ($mg \cdot m^{-2}$) were retrieved from the inversion of the Soil Canopy Observation of Photosynthesis and Energy fluxes (SCOPE) model [39]. The upper and lower boundaries and the initial values were set as per Rastogi et al. [40] (Supplementary Materials S1: Table S4). The LAI is one of the directly retrieved parameters from SCOPE inversion, while CCC was calculated as a product of LAI and leaf chlorophyll content.

2.5. Vegetation and Land Surface Phenology Retrieval

Decomposition and Analysis of Time Series Software (DATimeS, Version:1.10) was used for the phenology retrieval [41]. Because of the discontinuous dataset for hyperspectral reflectance-derived parameters, their time series were firstly gap-filled using the Whittaker-Henderson method in DATimeS. The smoothing parameter was set to 1000 for NDVI, 500 for NIRv, EVI, PPI, GCC, and ExG, and 100 for MTCI, LAI, and CCC. The start of the season (SoS) and the end of the season (EoS) were then retrieved using the threshold method with a seasonal amplitude of 20%, which was indicated as performing well for vegetation with an unorthodox phenology, including wetlands [11,30]. Minimal prominence was set to 20%, and minimal separation was set to 100 days. The peak of the season (PoS) was identified as the day when the value of a particular metric was the highest.

GPP-derived phenological parameters were retrieved based on sunny days only. This is because GPP is largely dependent on incident PAR, and the plant biomass can realize its potential only when enough light is available. The sunny days were filtered based on the midday diffused-to-direct PAR ratio, which was set to below 0.35. The subsequent gap-filling and phenological parameters estimation was carried out as described above with a smoothing parameter of 1000 for gap-filling and a threshold of 30% of seasonal amplitude for SoS and EoS retrieval. The 30% threshold was used instead of 20% because, unlike the greenness of evergreen ecosystems, GPP drops to 0 during winter, and 20% amplitude is reached before any actual growth of the plants. The threshold above 20% of the seasonal amplitude for GPP was found to correspond to the VI-derived LSP in the boreal forest in the previous study [42].

The gap-filled time series of VIs, LAI, and CCC were multiplied by the daily average PAR to obtain the NDVIP, NIRvP, EVIP, PPIP, GCCP, ExGP, MTCIP, LAIP, and CCCP [43]. These were calculated to evaluate the predictive power of vegetation greenness-related parameters combined with PAR. As for GPP, the time series was filtered for sunny days only and gap-filled with a smoothing parameter of 1000. The gap-filled time series of sunny days PAR was obtained in the same manner. Phenological parameters were retrieved for VIs, LAI, and CCC.

The phenology retrieved from GPP was used as a control for changes in canopy photosynthetic activity, and CCC-derived LSP served as a control for canopy greenness and structure.

2.6. Statistical Analysis

The correlation coefficient and the significance of correlation were assessed in terms of simple linear regression. The differences in the performance of the remote sensing metrics in LSP retrieval accuracy were tested by the Friedman test followed by the Conover test. The impact of climate manipulation, the vegetation community, and the year were tested by linear mixed models, always examining one of the factors as fixed and the other two as random effects. All statistical analyses were carried out in RStudio version 2022.02.0+443 (RStudio Inc., Boston, MA, USA).

3. Results

3.1. Climatic Conditions and Changes Induced by Climate Manipulation

The year 2019 was an extremely warm year, with an average yearly temperature (measured 30 cm above ground) of 9.7 °C and 9.8 °C at the CL and CR sites, respectively. 2021 was a normal year considering the long-term average temperature for the location when the average yearly temperature at the CL site was 8.0 °C and 8.1 °C at the CR site. There was only one month with an average temperature below 0 °C in 2019, while there were three such months in 2021. Interestingly, the average temperature in May and September, the months at the edges of the main vegetation season, was the same (May) or even higher (September) in 2021 compared to 2019 (Supplementary Materials S1: Tables S5 and S6).

As the daytime W was induced passively by OTCs, the impact of W was stronger in summer when the days are longer and more direct radiation reaches the ground compared to winter for both sites and both years. At the CL site, W increased the average annual temperature by 0.6 °C and 0.4 °C in 2019 and 2021, respectively. The temperature of the WP plots was 0.3 °C and 0.6 °C higher in 2019 and 2021, respectively. W and WP of the CR site caused an increase in average annual temperature in 2019 by 0.4 °C and 0.6 °C, respectively. In 2021, the temperature of W and WP plots at the CR site was 0.7 °C higher than C (Supplementary Materials S1: Tables S5 and S6).

The precipitation amount was very similar in both years, with 545.2 mm in 2019 and 532.0 mm in 2021. In 2019, April and June were months characterized by low precipitation, while in 2021, precipitation in September was very low. The annual precipitation reduction due to rain curtain use in WP conditions was 11% in 2019 and 12% in 2021. Precipitation reduction was restricted to the spring-autumn period, with no reduction in the winter months (Supplementary Materials S1: Table S7).

3.2. Vegetation Indices-Based Land Surface Phenology Evaluation

The linear model between GPP-derived phenological parameters and the LSP parameters derived from reflectance-based parameters yielded significant correlations ($p < 0.05$) for SoS obtained from MTCI, GCC, CCCP, ExG, ExGP, PPIP, PPI, and NIRvP; PoS from MTCI,

CCC, and PAR; and EoS from MTCI, CCCP, and CCC (Figure 2A). The correlation coefficient over 0.5 was recorded for SoS retrieved from the MTCI, ExGP, and ExG time-series and EoS from the MTCI and CCCP time series (Figure 2A).

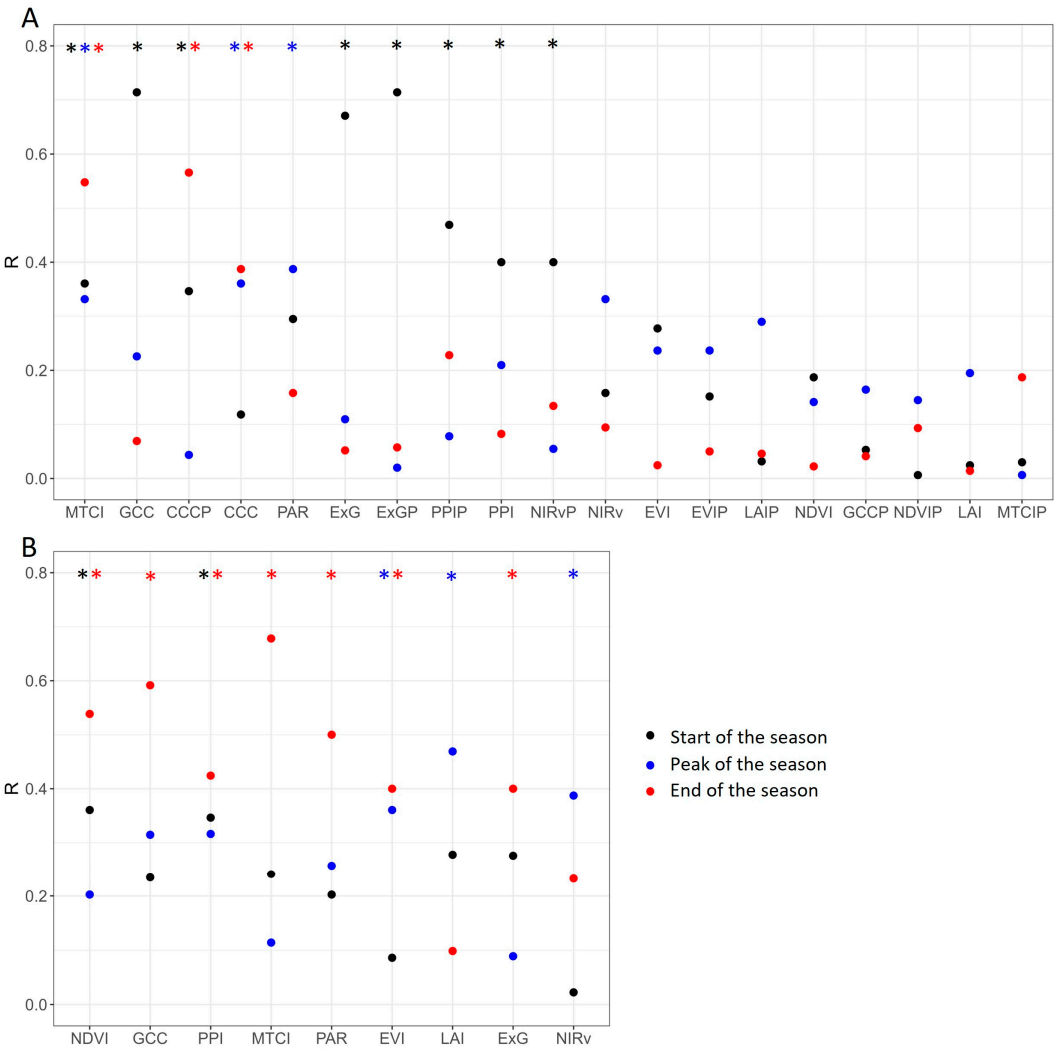


Figure 2. Correlation coefficient (R) for the linear model between gross primary production-derived (**A**) or canopy chlorophyll content-derived (**B**) phenological parameters and the phenological parameters derived from different reflectance-based parameters. All observations, regardless of site, treatment, and year, were analyzed together (n = 72). The stars of a particular color indicate a significant correlation at alpha = 0.05. CCC—Canopy Chlorophyll Content, EVI—Enhanced Vegetation Index, ExG—Excess Green, GCC—Green Chromatic Coordinates, LAI—Leaf Area Index, MTCI—MERRIS Terrestrial Chlorophyll Index, NDVI—Normalized Difference Vegetation Index, NIRv—Near-Infrared Reflectance of Vegetation, PAR—Photosynthetically Active Radiation, PPI—Plant Phenology Index, CCCP—CCC*PAR, EVIP—EVI*PAR, ExGP—ExG*PAR, GCCP—GCC*PAR, LAIP—LAI*PAR, MTCIP—MTCI*PAR, NDVIP—NDVI*PAR, NIRvP—NIRv*PAR, PPIP—PPI*PAR.

SoS derived from NDVI and PPI correlated significantly with SoS based on CCC, while for PoS, a significant correlation with CCC was found for EVI, LAI, and ExG. EoS derived from all metrics except LAI and NIRv correlated significantly with CCC-based EoS (Figure 2B). The correlation coefficient between CCC-based LSP and a remote sensing LSP higher than 0.5 was found only for EoS derived from NDVI, GCC, and MTCI (Figure 2B).

The simple VI with the lowest mean absolute error (MAE) in SoS compared to GPP-derived SoS was found to be ExG with an error of 15.1 days (Figure 3A). However, the

best performing of all evaluated remote sensing metrics for physiological SoS retrieval was NIRvP with an MAE of 13.4 days. It is important to note that despite the fact that the MAE was the lowest for NIRvP, the performance of NIRvP was not statistically significantly different from EVIP, CCCP, NDVIP, GCCP, LAIP, MTCIP, or the already mentioned ExG (Figure 3A). The lowest MAE for physiological PoS retrieval was recorded for ExGP, with NIRvP, EVIP, CCCP, NDVIP, GCCP, MTCIP, PPIP, and PPI not performing significantly differently (Figure 3A). EoS retrieval was characterized by the lowest MAE of all the LSP parameters, with a value of 8.8 for CCCP and below 10 for NIRvP, EVIP, NDVIP, and GCCP. The majority of the studied remote sensing metrics did not perform significantly worse than CCCP (Figure 3A). It is evident that PAR had a strong role in EoS estimation when EoS derived from PAR itself reached MAE 10.3. Among the simple VIs, PPI had the lowest MAE for PoS and EoS.

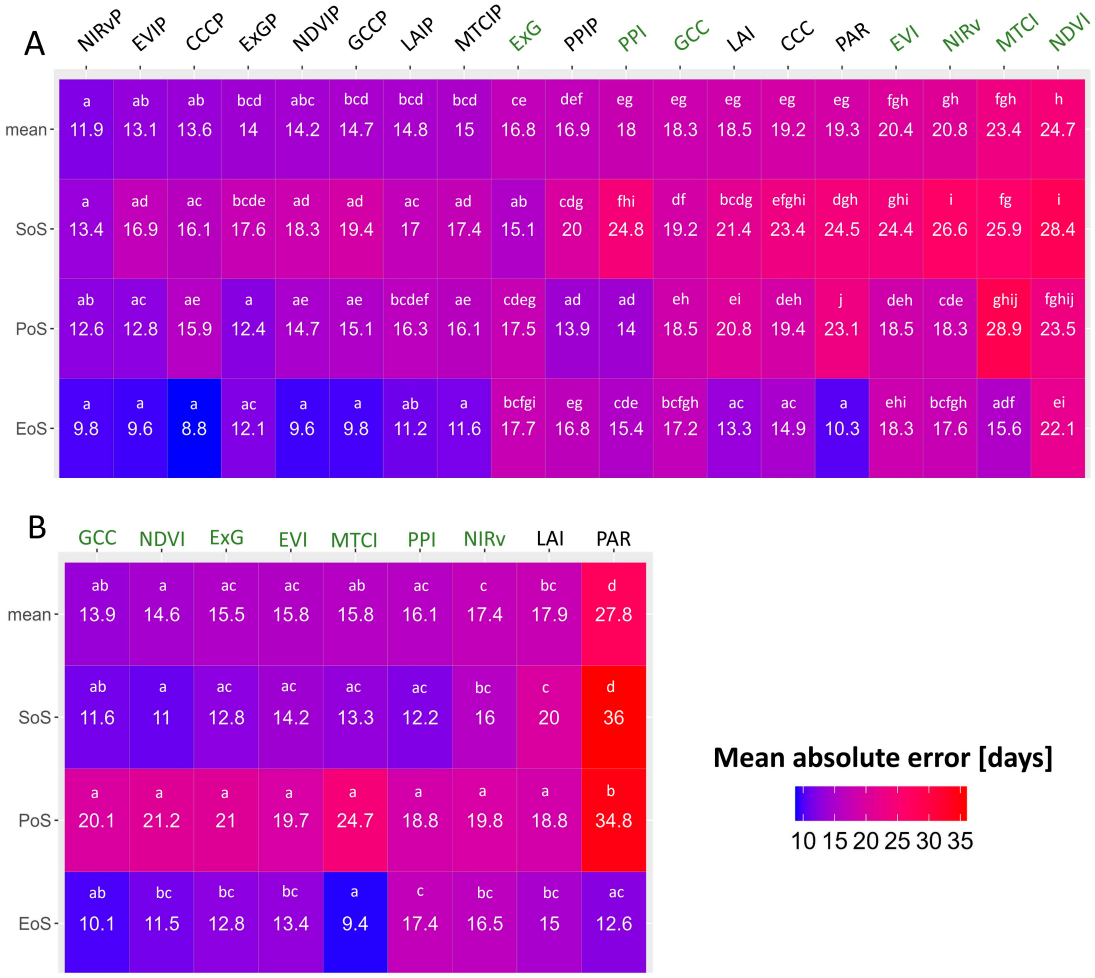


Figure 3. The mean absolute error of chosen remote sensing metrics-derived gross primary production-based (**A**) and canopy chlorophyll content-based (**B**) start of the season (SoS), peak of the season (PoS), end of the season (EoS), and the general performance calculated as the mean of SoS, PoS, and EoS (mean). Different letters within the cells of the same parameter (SoS, PoS, Eos, or mean) denote significantly different performances at alpha = 0.05, as found by the Conover test. Green names of metrics denote the simple vegetation indices. CCC—Canopy Chlorophyll Content, EVI—Enhanced Vegetation Index, ExG—Excess Green, GCC—Green Chromatic Coordinates, LAI—Leaf Area Index, MTCI—MERRIS Terrestrial Chlorophyll Index, NDVI—Normalized Difference Vegetation Index, NIRv—Near-Infrared Reflectance of Vegetation, PAR—Photosynthetically Active Radiation, PPI—Plant Phenology Index, CCCP—CCC*PAR, EVIP—EVI*PAR, ExGP—ExG*PAR, GCCP—GCC*PAR, LAIP—LAI*PAR, MTCIP—MTCI*PAR, NDVIP—NDVI*PAR, NIRvP—NIRv*PAR, PPIP—PPI*PAR.

Judging the overall performance of remote sensing metrics in physiological phenology estimation as an average of SoS, PoS, and EoS MAEs, ExG reached the lowest MAE among simple VIs and NIRvP out of all the evaluated remote sensing metrics. The performance of EVIP, CCCP, and NDVIP was not significantly worse than NIRvP. Among simple VIs, PPI and GCC were not significantly worse than ExG. The worst performance for GPP-based phenology estimation was recorded for NDVI, with MTCI, NIRv, and EVI not performing significantly differently (Figure 3A).

Contrary to GPP-based SoS, NDVI had the lowest MAE for estimating CCC-derived SoS with a value of 11.0, with all VIs except NIRv performing similarly (Figure 3B). VIs had low predictive power for CCC-derived PoS estimation when the best-performing VI, PPI, reached MAE at 18.8 days. All of the remote sensing metrics performed statistically equally in structural PoS retrieval (Figure 3B). The lowest MAE for structural EoS estimation was recorded for MTCI, with a value of 9.4, and with GCC and PAR not performing significantly differently (Figure 3B). As expected, PAR-derived and CCC-based SoS and PoS were not related. However, a surprisingly low MAE (12.6) was recorded for PAR-derived EoS. Generally, the best-performing VI for structural phenology estimation was GCC with MAE 13.9, but only NIRv performed statistically significantly worse (Figure 3B).

3.3. Gross Primary Production and Canopy Chlorophyll Content-Based Vegetation Phenology

The physiological vegetation season of plots without manipulation started on the day of the year (DoY) 107 (±14.6). W caused 11.8 (±3.9) days, and WP caused 10.3 (±3.9) days advance in the onset of the GPP-derived vegetation season (Table 1A). The physiological PoS of C plots occurred at DoY 197 (±5.2) with insignificant changes due to W, but 11 (±4.3) days sooner PoS was caused by WP. In general, the season ended at DoY 281 (±8.2), with no significant impact of climate manipulation. The physiological vegetation season of C plots was 174 (±21.8) days long, with significant prolongation by 16.4 (±5.8) and 11.6 (±5.8) days due to W and WP, respectively (Table 1A). The structural season of peatland vegetation started, peaked, and ended later than its physiological season. The structural season of C plots began on DoY 118 (±4.5), peaked on DoY 203 (±8.2), and finished on DoY 296 (±10.5). The season lasted for 178 (±14.5) days. No significant shifts caused by climate manipulation were recorded (Table 1B).

Table 1. Results of the mixed linear model presenting the differences among treatments (fixed effect) for phenological parameters derived from gross primary production (**A**) and canopy chlorophyll content (**B**) time series. Significant differences with $t > |2|$ are highlighted in bold. C—control, ΔW-C—the difference between warming and control, ΔWP-C—the difference between warming and reduced precipitation and control, Est.—estimate, SE—standard error, *t*—*t*-value, SoS—start of season, PoS—peak of season, EoS—end of season, LoS—length of season, n = 24.

A	**SoS**			**PoS**			**EoS**			**LoS**		
	Est.	**SE**	***t***	**Est.**	**SE**	***t***	**Est.**	**SE**	***t***	**Est.**	**SE**	***t***
C	107	14.6	7.34	197	5.2	37.87	281	8.2	34.19	174	21.8	7.96
ΔW-C	**−11.8**	**3.9**	**−2.99**	−4.3	4.3	−0.10	4.7	3.5	1.32	**16.4**	**5.8**	**2.84**
ΔWP-C	**−10.3**	**3.9**	**−2.63**	**−11.0**	**4.3**	**−2.58**	1.3	3.5	0.35	**11.6**	**5.8**	**2.00**
B												
	Est.	**SE**	***t***	**Est.**	**SE**	***t***	**Est.**	**SE**	***t***	**Est.**	**SE**	***t***
C	118	4.5	26.41	203	8.2	24.82	296	10.52	28.12	178	14.47	12.27
ΔW-C	5.0	5.8	0.86	1.92	9.5	0.20	0.83	5.7	0.15	−4.17	9.1	−0.46
ΔWP-C	−7.7	5.8	−1.32	−13.6	9.5	−1.44	−4.92	5.7	−0.86	2.75	9.1	0.30

The results of the mixed linear model for physiological phenology with treatment (C, W, WP) as a fixed effect suggest a strong random effect of the site (vegetation community) for LoS, SoS, and EoS, while the random effects on PoS and all phenometrics of structural phenology were not explained by the vegetation community or the year (Supplementary Materials S1: Table S8).

The physiological vegetation season generally started sooner and finished later at the CR site, where vegetation comprises more evergreen plants. While the season started on DoY 114 (±6.4) and ended on DoY 275 (±2.3) at the CL site, it started 27.1 (±3.2) days sooner and ended 15.8 (±2.9) days later at the CR site. The season was 162 (±6) days long at the CL site and 42.9 (±4.7) days longer at the CR site. The vegetation community had no significant effect on physiological PoS and structural SoS and PoS. The structural EoS occurred at the CL site on DoY 288 (±8.6) and at the CR site 12 (±4.6) days later. The LoS at the CL site was 168 (±11.8) days, and it was 17 (±7.3) days longer at the CR site.

The GPP-derived season started on DoY 95 (±14.1) in 2019, which was 11 (±3.2) days sooner than in 2021. PoS occurred at DoY 197 (± 3.6) in 2019 with 9 (±3.5) days advancement in 2021. The end of the physiological season was found at DoY 281 (±8), and the LoS was 187 (±22) days with no significant differences between years. The start and peak of structural season happened at DoY 114 (±4.4) and 193 (±6.2), respectively, without significant differences between years. The season ended on DoY 303 (±6.5) in 2019 and 17 (±4.6) days sooner in 2021. The CCC-derived season was 188 (±9.1) days long in 2019 and 23 (±7.3) days shorter in 2021.

4. Discussion

4.1. Evaluation of Remote Sensing for Peatland Phenology Assessment

The majority of LSP studies use the species-specific phenology observed by personal observations or ground-based sensors as a control for remote sensing phenology [7]. However, such observations can only be used for homogeneous vegetation and not for vegetation consisting of species with different phenologies [44]. LSP research on mixed vegetation phenology often uses flux tower GPP for inter-comparison. Nevertheless, this photosynthesis-based phenology is different from the traditional understanding of plant phenology, which is mostly connected to the changes in green biomass during the vegetative stages of ontogenesis [7,8]. Therefore, we used two kinds of "true" phenology: one based on GPP (physiological) and the other based on CCC (structural), which relates to the growth and development of the leaves [45].

NDVI and EVI are the most used VIs for LSP studies, assuming that one or the other is a well-suited VI for the purpose [7]. We found out that while they both perform well considering the structural phenology, the MAE for GPP-derived LSP was at the level of 20–25 days. Neither NDVI- nor EVI-derived phenology correlated significantly with the physiological phenology of peatland vegetation (Figure 2A). The general low correlation of remote sensing phenology with physiological phenology complies with the results of a previous study [1], which also found low correlations between VIs-based and GPP-derived phenology. The error of 3–4 weeks for NDVI and EVI SoS relative to GPP-derived SoS found in this study is in concordance with previous work carried out in forests [2]. PPI estimates the peatland physiological phenology significantly better than NDVI, but the improvement is not as pronounced as in the case of evergreen forests [13]. However, PPI was found to estimate PoS, with the lowest MAE for physiological and structural phenology (Figure 3A). The good performance for PoS may be caused by the formulation of PPI, which is logarithmic and considers the maximum value of the VI [13]. MTCI, which is a well-accepted chlorophyll-related VI, performed poorly in estimating physiological phenology in this study when its MAE was almost a week larger than the MAE of ExG (Figure 3). The

high MAE is surprising considering that SoS, PoS, and EoS derived from MTCI time series significantly correlated with physiological phenology (Figure 2A). This example shows that the correlation does not need to mean a good estimation of phenology. However, due to its relation with chlorophyll content, MTCI performed well for CCC-derived EoS estimation, being significantly better than other VIs except GCC (Figure 3B).

Previous studies focused on the GPP-based phenology estimation by phenocams found a good agreement between RGB VIs and physiological phenology in forests [46,47] and high similarity between GPP and GCC seasonal patterns in peatland [23,25]. We found that GCC and ExG-derived SoS significantly ($p < 0.05$) and highly ($R > 0.6$) correlated with the physiological SoS. ExG was the best-performing simple VI for SoS assessment, with significantly better performance than any other simple VI. This is probably because the spring peatland physiological phenology is considerably driven by evergreen plants, and ExG was previously found to perform well in relationship to GPP for evergreen vegetation [46]. Although the peak and end of the physiological season were estimated the most precisely from PPI time series, the performance of PPI was not significantly better than ExG (Figure 3A). Based on our results, GCC provides the most precise estimates of structural phenology. While most indices performed statistically equally, NIRv and PPI were significantly less accurate for estimating SoS and PoS, respectively (Figure 3B). Our findings support the high importance of both RGB indices (ExG and GCC) for peatland physiological and structural phenology assessment.

We observed that VIs estimate the structural phenology better than the physiological phenology. This was an expected result, as the "greenness" of the canopy is a better proxy of CCC than of the physiological processes [30]. However, the product of VIs and PAR shows improved estimation power for GPP-based LSP compared to VIs or PAR only (Figure 3). That is because GPP is a result of CCC and light interaction, not only the greenness [48].

Among the assessed remote sensing and canopy parameters, NIRvP had the lowest MAE for overall physiological phenology assessment, with statistically equal performance with EVIP, CCCP, and NDVIP. It has been shown before that NIRvP is an index well related to the physiological activity of plants [43]. In this study, we showed that the NIRvP time series is also valuable for the start, peak, and end of photosynthetic activity estimation. Therefore, NIRvP can be suggested as a simple proxy for northern peatland vegetation phenology of physiological activity if the data for PAR is available or can be reliably obtained from public sources such as Prediction Of Worldwide Energy Resources from National Aeronautics and Space Administration [49].

We did not find an advantage of using SCOPE inversion for peatland physiological phenology assessment. VIs calculated from multispectral reflectance perform statistically equal to hyperspectral reflectance-derived CCC (Figure 3A). However, SCOPE inversion had an irreplaceable role in our structural phenology evaluation.

4.2. Impact of Warming (W) and Warming and Reduced Precipitation (WP) on Vegetation Phenology

The majority of phenological studies suggest sooner SoS with rising temperature [29,50]. We found a significant advance of GPP-based SoS caused by W and WP conditions compared to C, which complies with the previously published results (Table 1A). However, only the physiological phenology of peatland vegetation was significantly affected by warmer conditions, with the shifts in structural phenology caused by W or WP not being statistically significant (Table 1). These results suggest a stronger impact of increased temperature on the onset of photosynthetic activity of peat mosses and bog cranberries than on the growth of the vegetation. Nonetheless, the lack of differences in CCC-based phenology may be caused by the discontinuous nature of the spectral data acquisition, which conceals the less prominent shifts.

Only WP conditions caused a significantly sooner occurring peak of physiological activity and substantial, albeit insignificant, advancement of structural PoS. This was most likely caused by faster drying of the moss capitula, which turn yellow sooner and decrease their photosynthetic activity when their surface dries [51]. Faster onset of peat moss summer depression shifts the peak of vegetation's photosynthetic activity when the decrease of carbon uptake by mosses is stronger than the increase of assimilation by vascular plants [52].

We did not record any significant changes in the timing of physiological or structural EoS (Table 1). As found before, EoS in the northern hemisphere depends on the length of the day rather than the temperature; therefore, only moderate changes in EoS are expected with climate warming [50]. Our results, which demonstrate a low MAE for PAR (10.3 days) and for the product of VIs and PAR (Figure 3), align well with these findings.

Due to the advanced physiological SoS, the W and WP conditions extended the growing season compared to C, resulting in approximately two additional weeks of photosynthetic activity. This extended activity can significantly enhance yearly carbon assimilation, positively impacting the carbon balance of peatlands. However, warmer conditions also lead to increased decomposition rates, which, although not covered in this study, must be considered when evaluating the impact of warming on the ecosystem's carbon balance [18].

The physiological season of CR vegetation started about 4 weeks earlier and finished about 2 weeks later than for CL vegetation (Table 2A). These results can be understood only in the context of dominant species on the sites. More evergreen shrubs and peat mosses, which begin and end their photosynthetic activity with lower temperatures, are present on the CR site, while more graminoids and deciduous species, that need to grow their leaves in spring and undergo leaf senescence in autumn, are on the CL site [19,21,32,53]. The delayed overall vegetation senescence is also apparent in structural phenology when the season ended significantly later, prolonging the LoS at the CR site (Table 2B). Despite the small distance between the 2 vegetation communities (about 50 m), the dominance of bog-like vegetation on the CR site caused a 6-week longer vegetation season, underscoring the importance of local hydrological and hydrochemical conditions for multiple aspects of plant life.

Table 2. Results of the mixed linear model presenting the differences among sites (vegetation communities; fixed effect) for phenological parameters derived from gross primary production (**A**) and canopy chlorophyll content (**B**) time series. Significant differences with $t > |2|$ are highlighted in bold. CL—CL site, ΔCR-CL—the difference between CR and CL sites, Est.—estimate, SE—standard error, *t*—*t*-value, SoS—start of season, PoS—peak of season, EoS—end of season, LoS—length of season, n = 36.

A	**SoS**			**PoS**			**EoS**			**LoS**		
	Est.	**SE**	***t***	**Est.**	**SE**	***t***	**Est.**	**SE**	***t***	**Est.**	**SE**	***t***
CL	114	6.4	17.62	192	5.6	34.33	275	2.3	118.09	162	6.0	27.11
ΔCR-CL	**−27.1**	**3.2**	**−8.43**	−0.1	3.5	−0.02	**15.8**	**2.9**	**5.48**	**42.9**	**4.7**	**9.01**
B												
	Est.	**SE**	***t***	**Est.**	**SE**	***t***	**Est.**	**SE**	***t***	**Est.**	**SE**	***t***
CL	120	4.7	25.27	198	7.8	25.27	288	8.6	33.57	168	11.8	14.27
ΔCR-CL	−4.5	4.7	−0.95	4	7.8	0.47	**12**	**4.6**	**2.64**	**17**	**7.3**	**2.29**

The warmer year 2019 (Supplementary Materials S1: Tables S5 and S6) caused a significantly sooner onset of physiological SoS and PoS and a later finishing of the structural season. However, only the structural season was significantly longer in 2019 compared

to 2021 (Table 3). The interannual variation of the temperature regimes proves the above-mentioned stronger effect of spring warming on the onset of physiological activity than on the beginning of green biomass growth. The late end of the structural season in 2019 was caused by an unusually warm end of the year with the average daily temperature keeping above 2 °C even in December (Supplementary Materials S1: Tables S5 and S6). As CCC was retrieved based on the canopy reflectance and not by destructive laboratory methods, it provides information about the active chlorophyll content rather than the total CCC. The amount of evergreen species active chlorophyll that was absorbing the light probably did not decrease rapidly as a result of relatively high autumn and early winter temperatures in 2019, prolonging the structural season [53]. However, daily GPP was not affected by the higher temperatures as much as CCC was due to shorter days and lower light intensity available for photosynthesis (Table 3).

Table 3. Results of the mixed linear model presenting the differences among years (fixed effect) for phenological parameters derived from gross primary production (**A**) and canopy chlorophyll content (**B**) time series. Significant differences with $t > |2|$ are highlighted in bold. Est.—estimate, SE—standard error, *t*—*t*-value, SoS—start of season, PoS—peak of season, EoS—end of season, LoS—length of season, n = 36.

A	**SoS**			**PoS**			**EoS**			**LoS**		
	Est.	**SE**	***t***	**Est.**	**SE**	***t***	**Est.**	**SE**	***t***	**Est.**	**SE**	***t***
2019	95	14.1	6.75	197	3.6	53.91	281	8.0	35.09	187	22.0	8.49
Δ2021–2019	**11**	**3.2**	**3.28**	**−9**	**3.5**	**−2.63**	4	2.9	1.27	−7	4.7	−1.46
B												
	Est.	**SE**	***t***	**Est.**	**SE**	***t***	**Est.**	**SE**	***t***	**Est.**	**SE**	***t***
2019	114	4.4	26.12	193	6.2	31.08	303	6.5	46.73	188	9.1	20.77
Δ2021–2019	6	4.7	1.26	12	7.7	1.58	**−17**	**4.6**	**−3.61**	**−23**	**7.3**	**−3.10**

5. Conclusions and Future Perspectives

In this study, we evaluated the performance of remote sensing metrics for the LSP estimation of peatland vegetation, which is specific in its plant functional types composition with a high share of peat mosses. We assessed the MAE of canopy reflectance and PAR-derived parameters relative to physiological (GPP-derived) and structural (CCC-based) LSP. Moreover, we studied the impact of climate on the different temperature and precipitation regimes and vegetation community on the peatland LSP.

The traditionally used VIs for satellite remote sensing of LSP, such as NDVI and EVI, were outperformed by RGB VI, ExG, in the estimation of physiological, GPP-based, peatland LSP. However, the product of simple VIs and PAR showed substantially lower MAE, and NIRvP, together with EVIP, were found as the best-performing indices for the physiological phenology assessment of peatlands. The structural phenology was estimated by remote sensing metrics more precisely than the physiological phenology. Although GCC was the index with the lowest MAE for structural phenology assessment, it performed statistically equal with NDVI, ExG, EVI, MTCI, and PPI.

Our results suggest that the changes in the physiological phenology due to W and WP are more prominent than the changes in structural phenology. This may mean that despite a rather accurate assessment of the structural LSP of peatland by remote sensing, the changes in the functioning of the ecosystem can be underestimated. This issue might be overcome by using sun-induced fluorescence from the upcoming FLuorescence EXplorer mission by the European Space Agency, which will have a spatial resolution suitable for monitoring ecosystems scattered in the landscape.

As only one LSP retrieval method was tested in this study, future work should focus on evaluating different methods. Including more years of observations and peatlands of different latitudes would further strengthen future work on peatland vegetation LSP.

Supplementary Materials: The following supporting information can be downloaded at: https://www.mdpi.com/article/10.3390/rs17010032/s1, Figure S1: Representative photographs of site; Table S1: Table of hyperspectral measurement campaigns with the campaign number in the calendar year.; Table S2: Reflectance-based vegetation indices used in this study; Table S3: Table of carbon dioxide flux measurement campaigns with the campaign number in the calendar year.; Table S4. Table of lower boundaries (LBs), upper boundaries (UBs), and initial values (IVs) for parameters retrieved by Soil Canopy Observation of Photosynthesis and Energy fluxes model inversion; Table S5. The average monthly and yearly temperature of control plots (T) and the impact of warming (ΔT W-C) and warming and reduced precipitation (ΔT WP-C) on the air temperature 30 cm above ground at the CL site in 2019 and 2021.; Table S6. The average monthly and yearly temperature of control plots (T) and the impact of warming (ΔT W-C) and warming and reduced precipitation (ΔT WP-C) on the air temperature 30 cm above ground at the CR site in 2019 and 2021.; Table S7. The sum of precipitation and the amount of precipitation reduction (ΔPrecipitation WP-C) in different months of 2019 and 2021.; Table S8. Results of the mixed linear model presenting the standard deviation of random effects caused by site, year and residual on the differences in phenological parameters derived from gross primary production (A) and canopy chlorophyll content (B) time series caused by treatment as the fixed effect.

Author Contributions: M.A.: conceptualization, data curation, formal analysis, investigation, methodology, visualization, and writing—original draft. A.R.: conceptualization, funding acquisition, project administration, supervision, formal analysis, investigation, and writing—review and editing. M.S.: data curation, investigation, supervision, and writing—review and editing. M.A.-S.: data curation, investigation and writing—review and editing. S.B.: data curation, investigation, and writing—review and editing. R.J.: conceptualization, resources, funding acquisition, project administration, supervision, formal analysis, investigation, and writing—review and editing. All authors have read and agreed to the published version of the manuscript.

Funding: This research was supported by the National Science Centre of Poland (NCN) within grants No. 2016/21/B/ST10/02271 and 2020/37/B/ST10/01213, and the Action CA17134 SENSECO (Optical synergies for spatiotemporal sensing of scalable ecophysiological traits) funded by COST (European Cooperation in Science and Technology).

Data Availability Statement: The raw data supporting the conclusions of this article will be made available by the authors on request.

Conflicts of Interest: The authors declare no conflict of interests.

References

1. Wu, C.; Peng, D.; Soudani, K.; Siebicke, L.; Gough, C.M.; Arain, M.A.; Bohrer, G.; Lafleur, P.M.; Peichl, M.; Gonsamo, A.; et al. Land Surface Phenology Derived from Normalized Difference Vegetation Index (NDVI) at Global FLUXNET Sites. *Agric. For. Meteorol.* **2017**, *233*, 171–182. [CrossRef]
2. Chang, Q.; Xiao, X.; Jiao, W.; Wu, X.; Doughty, R.; Wang, J.; Du, L.; Zou, Z.; Qin, Y. Assessing Consistency of Spring Phenology of Snow-Covered Forests as Estimated by Vegetation Indices, Gross Primary Production, and Solar-Induced Chlorophyll Fluorescence. *Agric. For. Meteorol.* **2019**, *275*, 305–316. [CrossRef]
3. Keenan, T.F.; Richardson, A.D.; Hufkens, K. On Quantifying the Apparent Temperature Sensitivity of Plant Phenology. *New Phytol.* **2020**, *225*, 1033–1040. [CrossRef]
4. Feller, C. The BBCH System to Coding the Phenological Growth Stages of Plants-History and Publications. *J. Fur Kult.* **2009**, *61*, 41–52. [CrossRef]
5. Zadoks, J.C.; Chang, T.T.; Konzak, C.F.; Fryer, J.D. A Decimal Code for the Growth Stages of Cereals. *Weed Res.* **1974**, *14*, 415–421. [CrossRef]

6. Hanes, J.M.; Liang, L.; Morisette, J.T. Land Surface Phenology. In *Biophysical Applications of Satellite Remote Sensing*; Hanes, J.M., Ed.; Springer: Berlin/Heidelberg, Germany, 2014; pp. 99–125, ISBN 978-3-642-25046-0.
7. Caparros-Santiago, J.A.; Rodriguez-Galiano, V.; Dash, J. Land Surface Phenology as Indicator of Global Terrestrial Ecosystem Dynamics: A Systematic Review. *ISPRS J. Photogramm. Remote Sens.* **2021**, *171*, 330–347. [CrossRef]
8. Berra, E.F.; Gaulton, R. Remote Sensing of Temperate and Boreal Forest Phenology: A Review of Progress, Challenges and Opportunities in the Intercomparison of in-Situ and Satellite Phenological Metrics. *For. Ecol. Manag.* **2021**, *480*, 118663. [CrossRef]
9. Shang, R.; Liu, R.; Xu, M.; Liu, Y.; Zuo, L.; Ge, Q. The Relationship between Threshold-Based and Inflexion-Based Approaches for Extraction of Land Surface Phenology. *Remote Sens. Environ.* **2017**, *199*, 167–170. [CrossRef]
10. Huang, X.; Liu, J.; Zhu, W.; Atzberger, C.; Liu, Q. The Optimal Threshold and Vegetation Index Time Series for Retrieving Crop Phenology Based on a Modified Dynamic Threshold Method. *Remote Sens.* **2019**, *11*, 2725. [CrossRef]
11. Xie, Q.; Moore, C.E.; Cleverly, J.; Hall, C.C.; Ding, Y.; Ma, X.; Leigh, A.; Huete, A. Land Surface Phenology Indicators Retrieved across Diverse Ecosystems Using a Modified Threshold Algorithm. *Ecol. Indic.* **2023**, *147*, 110000. [CrossRef]
12. Sonnentag, O.; Hufkens, K.; Teshera-Sterne, C.; Young, A.M.; Friedl, M.; Braswell, B.H.; Milliman, T.; O'Keefe, J.; Richardson, A.D. Digital Repeat Photography for Phenological Research in Forest Ecosystems. *Agric. For. Meteorol.* **2012**, *152*, 159–177. [CrossRef]
13. Jin, H.; Eklundh, L. A Physically Based Vegetation Index for Improved Monitoring of Plant Phenology. *Remote Sens. Environ.* **2014**, *152*, 512–525. [CrossRef]
14. Badgley, G.; Field, C.B.; Berry, J.A. Canopy Near-Infrared Reflectance and Terrestrial Photosynthesis. *Sci. Adv.* **2017**, *3*, e1602244. [CrossRef] [PubMed]
15. Dash, J.; Curran, P.J. The MERIS Terrestrial Chlorophyll Index. *Int. J. Remote Sens.* **2004**, *25*, 5403–5413. [CrossRef]
16. Gorham, E. Northern Peatlands: Role in the Carbon Cycle and Probable Responses to Climatic Warming. *Ecol. Appl.* **1991**, *1*, 182–195. [CrossRef] [PubMed]
17. van Breemen, N. How Sphagnum Bogs down Other Plants. *Trends Ecol. Evol.* **1995**, *10*, 270–275. [CrossRef]
18. Antala, M.; Juszczak, R.; van der Tol, C.; Rastogi, A. Impact of Climate Change-Induced Alterations in Peatland Vegetation Phenology and Composition on Carbon Balance. *Sci. Total Environ.* **2022**, *827*, 154294. [CrossRef] [PubMed]
19. Malmer, N.; Albinsson, C.; Svensson, B.M.; Wallén, B. Interferences between Sphagnum and Vascular Plants: Effects on Plant Community Structure and Peat Formation. *Oikos* **2003**, *100*, 469–482. [CrossRef]
20. Chiapusio, G.; Binet, P.; Bertheau, C.; Priault, P. Sphagnum Physiological Responses to Elevated Temperature, Nitrogen, CO_2 and Low Moisture in Laboratory and in Situ Microhabitats: A Review. *Aquat. Ecol.* **2021**, *8*, 429–445. [CrossRef]
21. Chapin, F.S.; Bret-Harte, M.S.; Hobbie, S.E.; Zhong, H. Plant Functional Types as Predictors of Transient Responses of Arctic Vegetation to Global Change. *J. Veg. Sci.* **1996**, *7*, 347–358. [CrossRef]
22. Buttler, A.; Robroek, B.J.M.; Laggoun-Défarge, F.; Jassey, V.E.J.; Pochelon, C.; Bernard, G.; Delarue, F.; Gogo, S.; Mariotte, P.; Mitchell, E.A.D.; et al. Experimental Warming Interacts with Soil Moisture to Discriminate Plant Responses in an Ombrotrophic Peatland. *J. Veg. Sci.* **2015**, *26*, 964–974. [CrossRef]
23. Linkosalmi, M.; Tuovinen, J.P.; Nevalainen, O.; Peltoniemi, M.; Taniş, C.M.; Arslan, A.N.; Rainne, J.; Lohila, A.; Laurila, T.; Aurela, M. Tracking Vegetation Phenology of Pristine Northern Boreal Peatlands by Combining Digital Photography with CO_2 flux and Remote Sensing Data. *Biogeosciences* **2022**, *19*, 4747–4765. [CrossRef]
24. Kross, A.S.E.; Roulet, N.T.; Moore, T.R.; Lafleur, P.M.; Humphreys, E.R.; Seaquist, J.W.; Flanagan, L.B.; Aurela, M. Phenology and Its Role in Carbon Dioxide Exchange Processes in Northern Peatlands. *J. Geophys. Res. Biogeosciences* **2014**, *119*, 1370–1384. [CrossRef]
25. Peichl, M.; Sonnentag, O.; Nilsson, M.B. Bringing Color into the Picture: Using Digital Repeat Photography to Investigate Phenology Controls of the Carbon Dioxide Exchange in a Boreal Mire. *Ecosystems* **2015**, *18*, 115–131. [CrossRef]
26. Koebsch, F.; Sonnentag, O.; Järveoja, J.; Peltoniemi, M.; Alekseychik, P.; Aurela, M.; Arslan, A.N.; Dinsmore, K.; Gianelle, D.; Helfter, C.; et al. Refining the Role of Phenology in Regulating Gross Ecosystem Productivity across European Peatlands. *Glob. Chang. Biol.* **2020**, *26*, 876–887. [CrossRef]
27. Dronova, I.; Taddeo, S.; Hemes, K.S.; Knox, S.H.; Valach, A.; Oikawa, P.Y.; Kasak, K.; Baldocchi, D.D. Remotely Sensed Phenological Heterogeneity of Restored Wetlands: Linking Vegetation Structure and Function. *Agric. For. Meteorol.* **2021**, *296*, 108215. [CrossRef]
28. Pang, Y.; Huang, Y.; He, L.; Zhou, Y.; Sui, J.; Xu, J. Remote Sensing Phenology of Two Chinese Northern Sphagnum Bogs under Climate Drivers during 2001 and 2018. *Ecol. Indic.* **2021**, *129*, 107968. [CrossRef]
29. Hufkens, K.; Friedl, M.; Sonnentag, O.; Braswell, B.H.; Milliman, T.; Richardson, A.D. Linking Near-Surface and Satellite Remote Sensing Measurements of Deciduous Broadleaf Forest Phenology. *Remote Sens. Environ.* **2012**, *117*, 307–321. [CrossRef]
30. Karkauskaite, P.; Tagesson, T.; Fensholt, R. Evaluation of the Plant Phenology Index (PPI), NDVI and EVI for Start-of-Season Trend Analysis of the Northern Hemisphere Boreal Zone. *Remote Sens.* **2017**, *9*, 485. [CrossRef]

31. Górecki, K.; Rastogi, A.; Stróżecki, M.; Gąbka, M.; Lamentowicz, M.; Łuców, D.; Kayzer, D.; Juszczak, R. Water Table Depth, Experimental Warming, and Reduced Precipitation Impact on Litter Decomposition in a Temperate Sphagnum-Peatland. *Sci. Total Environ.* **2021**, *771*, 145452. [CrossRef] [PubMed]
32. Antala, M.; Rastogi, A.; Cogliati, S.; Stróżecki, M.; Colombo, R.; Juszczak, R. Sun-Induced Fluorescence Spectrum as a Tool for Assessing Peatland Vegetation Productivity in the Framework of Warming and Reduced Precipitation Experiment. *Remote Sens. Environ.* **2024**, *301*, 113921. [CrossRef]
33. Rouse, J.W.; Haas, R.H.; Schell, J.A.; Deering, D.W. Monitoring Vegetation Systems in the Great Plains with ERTS. In Proceedings of the Third Earth Resources Technology Satellite–1 Symposium. Volume I: Technical Presentations, Washington, DC, USA, 10–14 December 1973; Freden, S.C., Mercanti, E.P., Becker, M., Eds.; NASA: Washington, DC, USA, 1974; pp. 309–317.
34. Liu, H.Q.; Huete, A. A Feedback Based Modification of the NDVI to Minimize Canopy Background and Atmospheric Noise. *IEEE Trans. Geosci. Remote Sens.* **1995**, *33*, 457. [CrossRef]
35. Acosta, M.; Juszczak, R.; Chojnicki, B.; Pavelka, M.; Havránková, K.; Lesny, J.; Krupková, L.; Urbaniak, M.; Machačová, K.; Olejnik, J. CO_2 Fluxes from Different Vegetation Communities on a Peatland Ecosystem. *Wetlands* **2017**, *37*, 423–435. [CrossRef]
36. Juszczak, R.; Uździcka, B.; Stróżecki, M.; Sakowska, K. Improving Remote Estimation of Winter Crops Gross Ecosystem Production by Inclusion of Leaf Area Index in a Spectral Model. *PeerJ* **2018**, *6*, e5613. [CrossRef]
37. Hoffmann, M.; Jurisch, N.; Albiac Borraz, E.; Hagemann, U.; Drösler, M.; Sommer, M.; Augustin, J. Automated Modeling of Ecosystem CO_2 Fluxes Based on Periodic Closed Chamber Measurements: A Standardized Conceptual and Practical Approach. *Agric. For. Meteorol.* **2015**, *200*, 30–45. [CrossRef]
38. Sakowska, K.; Alberti, G.; Genesio, L.; Peressotti, A.; Delle Vedove, G.; Gianelle, D.; Colombo, R.; Rodeghiero, M.; Panigada, C.; Juszczak, R.; et al. Leaf and Canopy Photosynthesis of a Chlorophyll Deficient Soybean Mutant. *Plant Cell Environ.* **2018**, *41*, 1427–1437. [CrossRef] [PubMed]
39. Van Der Tol, C.; Verhoef, W.; Timmermans, J.; Verhoef, A.; Su, Z. An Integrated Model of Soil-Canopy Spectral Radiances, Photosynthesis, Fluorescence, Temperature and Energy Balance. *Biogeosciences* **2009**, *6*, 3109–3129. [CrossRef]
40. Rastogi, A.; Antala, M.; Prikaziuk, E.; Yang, P.; van der Tol, C.; Juszczak, R. Exploring the Potential of SCOPE Model for Detection of Leaf Area Index and Sun-Induced Fluorescence of Peatland Canopy. *Remote Sens.* **2022**, *14*, 4010. [CrossRef]
41. Belda, S.; Pipia, L.; Morcillo-Pallarés, P.; Rivera-Caicedo, J.P.; Amin, E.; De Grave, C.; Verrelst, J. DATimeS: A Machine Learning Time Series GUI Toolbox for Gap-Filling and Vegetation Phenology Trends Detection. *Environ. Model. Softw.* **2020**, *127*, 104666. [CrossRef]
42. Gonsamo, A.; Chen, J.M.; D'Odorico, P. Deriving Land Surface Phenology Indicators from CO_2 Eddy Covariance Measurements. *Ecol. Indic.* **2013**, *29*, 203–207. [CrossRef]
43. Dechant, B.; Ryu, Y.; Badgley, G.; Köhler, P.; Rascher, U.; Migliavacca, M.; Zhang, Y.; Tagliabue, G.; Guan, K.; Rossini, M.; et al. NIRVP: A Robust Structural Proxy for Sun-Induced Chlorophyll Fluorescence and Photosynthesis across Scales. *Remote Sens. Environ.* **2022**, *268*, 112763. [CrossRef]
44. Doktor, D.; Bondeau, A.; Koslowski, D.; Badeck, F.W. Influence of Heterogeneous Landscapes on Computed Green-up Dates Based on Daily AVHRR NDVI Observations. *Remote Sens. Environ.* **2009**, *113*, 2618–2632. [CrossRef]
45. Graf, L.V.; Merz, Q.N.; Walter, A.; Aasen, H. Insights from Field Phenotyping Improve Satellite Remote Sensing Based In-Season Estimation of Winter Wheat Growth and Phenology. *Remote Sens. Environ.* **2023**, *299*, 113860. [CrossRef]
46. Toomey, M.; Friedl, M.A.; Frolking, S.; Hufkens, K.; Klosterman, S.; Sonnentag, O.; Baldocchi, D.D.; Bernacchi, C.J.; Biraud, S.C.; Bohrer, G.; et al. Greenness Indices from Digital Cameras Predict the Timing and Seasonal Dynamics of Canopy-Scale Photosynthesis. *Ecol. Appl.* **2015**, *25*, 99–115. [CrossRef] [PubMed]
47. Seyednasrollah, B.; Bowling, D.R.; Cheng, R.; Logan, B.A.; Magney, T.S.; Frankenberg, C.; Yang, J.C.; Young, A.M.; Hufkens, K.; Arain, M.A.; et al. Seasonal Variation in the Canopy Color of Temperate Evergreen Conifer Forests. *New Phytol.* **2021**, *229*, 2586–2600. [CrossRef]
48. Gu, L.; Han, J.; Wood, J.D.; Chang, C.Y.Y.; Sun, Y. Sun-Induced Chl Fluorescence and Its Importance for Biophysical Modeling of Photosynthesis Based on Light Reactions. *New Phytol.* **2019**, *223*, 1179–1191. [CrossRef] [PubMed]
49. Prediction Of Worldwide Energy Resources from National Aeronautics and Space Administration. Available online: https://power.larc.nasa.gov/data-access-viewer (accessed on 17 December 2024).
50. Descals, A.; Verger, A.; Yin, G.; Filella, I.; Fu, Y.H.; Piao, S.; Janssens, I.A.; Peñuelas, J. Radiation-Constrained Boundaries Cause Nonuniform Responses of the Carbon Uptake Phenology to Climatic Warming in the Northern Hemisphere. *Glob. Chang. Biol.* **2023**, *29*, 719–730. [CrossRef] [PubMed]
51. Gerdol, R.; Bonora, A.; Gualandri, R.; Pancaldi, S. CO, Exchange, Photosynthetic Pigment Composition, and Cell Ultrastructure of Sphagnum Mosses during Dehydration and Subsequent Rehydration. *Can. J. Bot.* **1996**, *74*, 726–734. [CrossRef]

52. Radu, D.; Duval, T. Precipitation Frequency Alters Peatland Ecosystem Structure and CO_2 Exchange: Contrasting Effects on Moss, Sedge, and Shrub Communities. *Glob. Chang. Biol.* **2018**, *24*, 2051–2065. [CrossRef]
53. Lundell, R.; Saarinen, T.; Åström, H.; Hänninen, H. The Boreal Dwarf Shrub Vaccinium Vitis-Idaea Retains Its Capacity for Photosynthesis through the Winter. *Botany* **2008**, *86*, 491–500. [CrossRef]

Disclaimer/Publisher's Note: The statements, opinions and data contained in all publications are solely those of the individual author(s) and contributor(s) and not of MDPI and/or the editor(s). MDPI and/or the editor(s) disclaim responsibility for any injury to people or property resulting from any ideas, methods, instructions or products referred to in the content.